Research Square

Preprints are preliminary reports that have not undergone peer review.
They should not be considered conclusive, used to inform clinical practice,
or referenced by the media as validated information.

Controls on Gold Mineralisation in the Tamar Area, North Singhbhum Mobile Belt, Eastern India

Mr. Kalyan Pal

kalyan.pal@gsi.gov.in

Central University of Punjab

Prof. A. S. Venkatesh

Indian Institute of Technology Dhanbad

Dr. Rahul Mukherjee

Central University of Punjab

Research Article

Keywords: Orogenic gold, North Singhbhum Mobile Belt, Shear zones, Fluid inclusions, Paleoproterozoic mineralization

Posted Date: May 26th, 2026

DOI: https://doi.org/10.21203/rs.3.rs-9266450/v1

License: This work is licensed under a Creative Commons Attribution 4.0 International License.
Read Full License

Additional Declarations:
No competing interests reported.

Tables 1 to 3 are available in the supplementary files section

Controls on Gold Mineralisation in the Tamar Area, North Singhbhum Mobile Belt, Eastern India

Kalyan Pal[1]*, A. S. Venkatesh[2], Rahul Mukherjee[3]
1 Research Scholar, Department of Geology, Central University of Punjab, Bathinda- 151401, India
2 Department of Applied Geology, Indian Institute of Technology (Indian School of Mines), Dhanbad 826004, India. asvenkatesh@hotmail.com
3 Department of Geology, Central University of Punjab, Bathinda 151401, India. rahul.mukherjee@cup.edu.in
*Corresponding author: kalyan.pal@gsi.gov.in

Abstract

The North Singhbhum Mobile Belt (NSMB), forming the southern tectonic margin of the Chhotanagpur Gneissic Complex (CGGC), represents a Paleoproterozoic orogenic belt with significant but underexplored gold potential. This study integrates field geology, structural analysis, petrography, whole-rock geochemistry, fluid inclusion microthermometry, and Raman spectroscopy to constrain the lithological, structural, metamorphic, and physicochemical controls on gold mineralisation in the Tamar area.

Gold occurs as disseminations and quartz–carbonate vein systems hosted within quartzite, limonitic quartzite, carbonaceous phyllite, and amphibolite, spatially associated with WNW–ESE-trending ductile to brittle–ductile shear zones linked to the South Purulia Shear Zone. Structural traps such as shear intersections, fold hinges, and lithological contacts exert primary control on ore localisation. Fluid inclusion studies reveal low- to moderate-salinity aqueous–carbonic fluids (CO_2–CH_4–H_2O ± NaCl) with homogenization temperatures of ~245–370 °C. Raman spectroscopy confirms reduced fluid compositions containing CO_2, CH_4, graphite, and minor H_2S.

These features indicate metamorphic fluid derivation, with gold transported as bisulfide complexes and precipitated through fluid immiscibility, sulfidation, and redox reactions. The Tamar gold system is interpreted as a Paleoproterozoic mesothermal (orogenic) gold deposit formed during late-stage deformation in a convergent tectonic regime. This study establishes a robust genetic framework and highlights the metallogenic potential of the NSMB.

Keywords: Orogenic gold; North Singhbhum Mobile Belt; Shear zones; Fluid inclusions; Paleoproterozoic mineralization.

1. Introduction

Orogenic gold deposits constitute a major class of hydrothermal gold systems globally and are typically associated with convergent tectonic environments, crustal shortening, and large-scale shear zones (Groves et al., 2003, 2018; Goldfarb and Groves, 2015; Goldfarb et al., 2005). These deposits form at mid-crustal depths (~5–15 km) under greenschist to amphibolite facies

conditions and are characterised by structurally focused fluid flow and deformation-driven permeability (Phillips and Powell, 2010; Groves et al., 2020).

Recent advances emphasise the role of: episodic fault-valve behaviour (Sibson et al., 1988; Cox, 2005; Cox et al., 2020), dynamic fluid pressure fluctuations (Weatherley and Henley, 2013), and fluid–rock interaction processes (Ridley and Diamond, 2000; Kerrich et al., 2000).

Gold transport occurs predominantly as Au–HS complexes in reduced, CO_2-rich metamorphic fluids (Seward, 1997; Gammons and Williams-Jones, 1997), whereas precipitation is triggered by pressure drop, fluid immiscibility, sulfidation, and redox changes (Tomkins and Mavrogenes, 2001; Gaboury, 2019).

In the Indian context, Paleoproterozoic mobile belts such as the NSMB represent promising but underexplored metallogenic provinces (Santosh et al., 2017; Deng et al., 2019). Despite occurrences of auriferous quartz veins in the Tamar region, the controls on mineralisation remain poorly constrained.

This study aims to: 1. Characterise lithological and structural controls. 2. Constrain fluid composition and evolution. 3. Develop a genetic model 4. Compare Tamar with global orogenic gold systems

2. Geological Setting

The Tamar area is situated along the southern margin of the CGGC and forms part of the Paleoproterozoic NSMB, representing a tectonically reworked supracrustal sequence within the Singhbhum crustal province. The belt comprises volcano-sedimentary assemblages intruded by granitoids and alkaline bodies and is tectonically juxtaposed against the Singhbhum Group along the South Purulia Shear Zone, a major crustal-scale structure active during Paleoproterozoic orogenesis. The NSMB is a Paleoproterozoic mobile belt developed along the southern margin of the CGGC and represents a tectonically reworked volcano-sedimentary sequence intruded by granitoids (Zhai and Santosh, 2011; Santosh et al., 2017).

The regional geology reflects a polyphase tectono-metamorphic history involving repeated episodes of compression, transpression, and shearing, resulting in the development of penetrative foliations, mylonitic fabrics, and shear-controlled fluid pathways. Metamorphism reached greenschist to amphibolite facies conditions, consistent with typical orogenic gold environments (Groves et al., 1998; Kerrich et al., 2000).

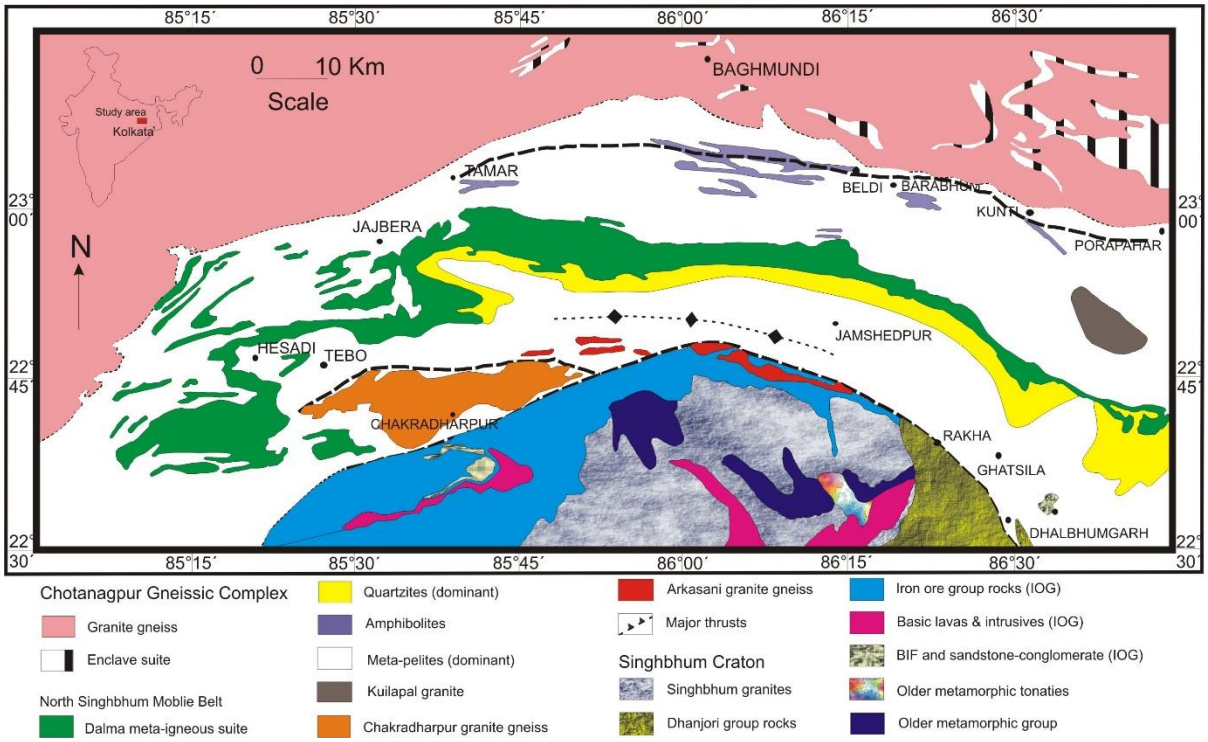


Fig. 1. Location and geological map of the study area. (Source: Geological Survey of India)

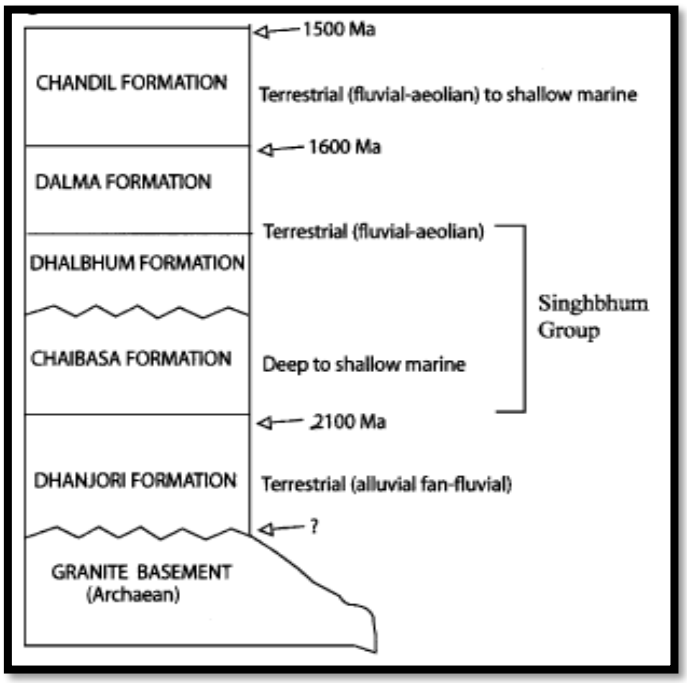


Table 1. Revised Proterozoic stratigraphic succession of the Singhbhum crustal province (Mazumdar, R., 2005).

3. Lithological Characteristics

The supracrustal sequence in the study area comprises quartz-sericite mica schist, carbonaceous phyllite, limonitic quartzite, quartzite, amphibolite, and minor ultramafic lenses.

Carbonaceous phyllite and mica schist are the most extensive lithologies and locally grade into one another. Quartzite and limonitic quartzite form laterally persistent bands and constitute the principal hosts to gold mineralization.

Amphibolites, interpreted as metamorphosed mafic volcanic or intrusive protoliths, are locally mylonitized within shear zones. Ultramafic bodies, altered to talc–chlorite–tremolite assemblages, occur as discontinuous lenses within the supracrustal sequence. The preferential development of gold mineralization within quartzite, limonitic quartzite, carbonaceous phyllite, and amphibolite highlights the importance of lithological reactivity and competency contrasts in controlling ore deposition.

These lithologies exert control through: (a) competency contrasts, facilitating fracturing and fluid flow (Neumayr et al., 2008), (b) chemical reactivity, especially in Fe-rich rocks promoting sulfidation (Large et al., 2011), (c) carbonaceous matter, acting as a redox buffer (Tomkins, 2010). Such lithological control is widely recognised in orogenic gold systems worldwide (Hagemann and Cassidy, 2000; Dubé and Gosselin, 2007).

4. Structural Controls on Mineralisation

At least two major deformation events are recognised in the Tamar area. The dominant deformation phase produced a WNW–ESE to ENE–WSW-trending penetrative foliation (S_2) with steep dips, overprinting an earlier S_1 fabric. The S_2 foliation is defined by aligned sericite, muscovite, chlorite, and locally hornblende.

Gold mineralisation is spatially associated with ductile to brittle–ductile shear zones characterised by mylonitization, brecciation, silicification, and carbonatization. Quartz veins are preferentially emplaced parallel to foliation planes or within extensional sites generated during late-stage deformation. Structural traps include fold hinges, shear intersections, fault splays, and lithological contacts, which collectively focused hydrothermal fluid flow and gold precipitation.

Structural traps include: (a) fold hinges, (b) shear zone intersections and (c) fault splays. These structures create transient dilatant zones that enhance permeability and fluid flow (Micklethwaite et al., 2010; Cox et al., 2020). The observed structural framework supports a fault-valve model, where episodic fluid pressure release controls gold deposition (Sibson et al., 1988; Cox, 2005).

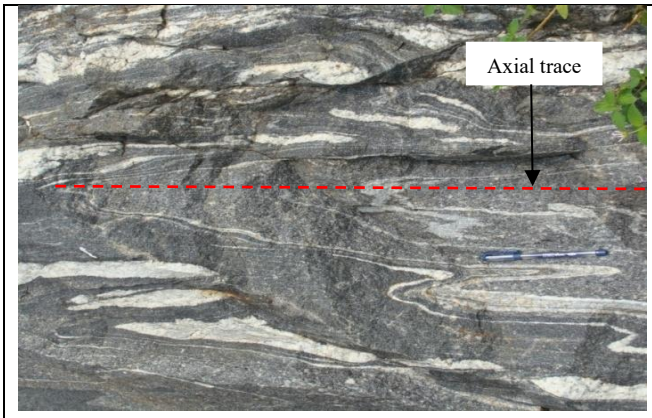


Fig. 2.(a) Field photograph showing plunging fold on the migmatised rock

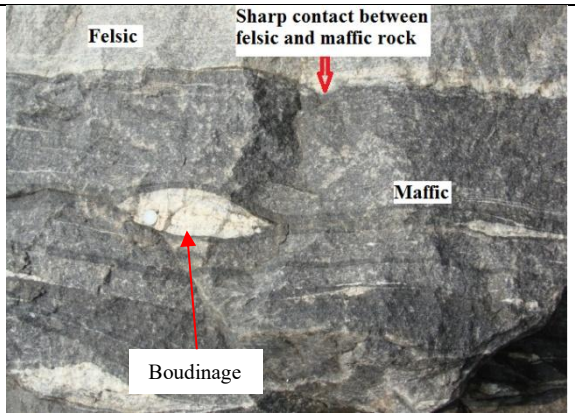


Fig. 2.(b) Field photograph showing sharp contact between felsic and mafic rock

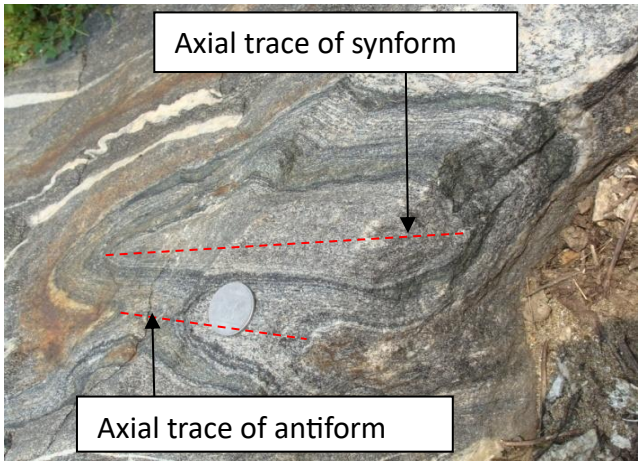


Fig. 2. (c) Field photograph showing non-plunging synform and antiform.

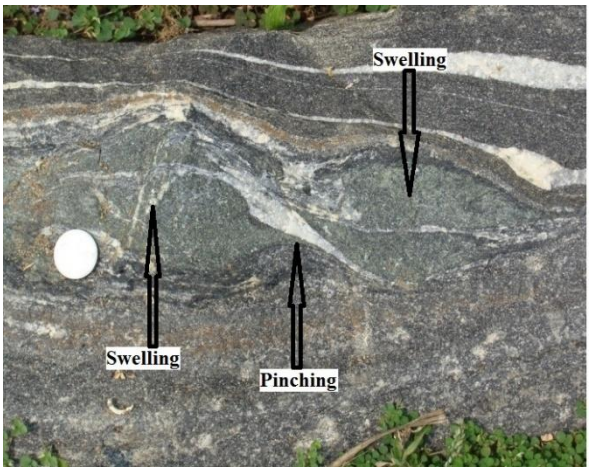


Fig. 2. (d) Field photograph showing pinch and swell.

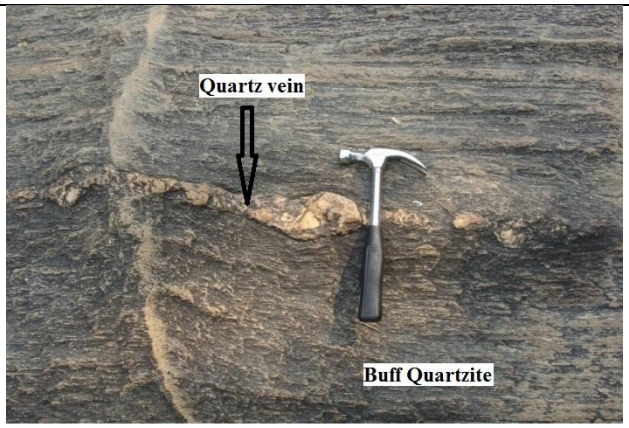


Fig. 2. (e) Field photograph showing quartz vein intruded in buff quartzite.

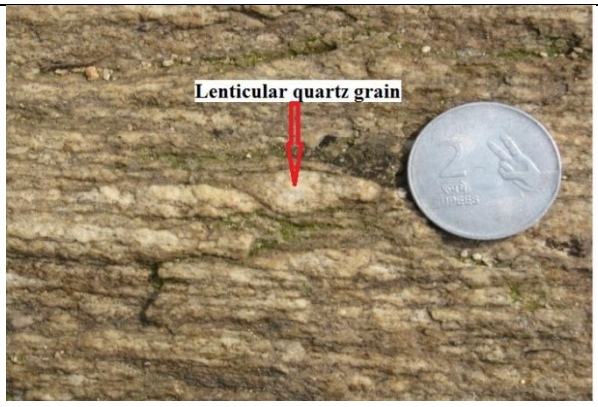


Fig. 2. (f) Field photograph showing lenticular quartz grain found in quartzite.

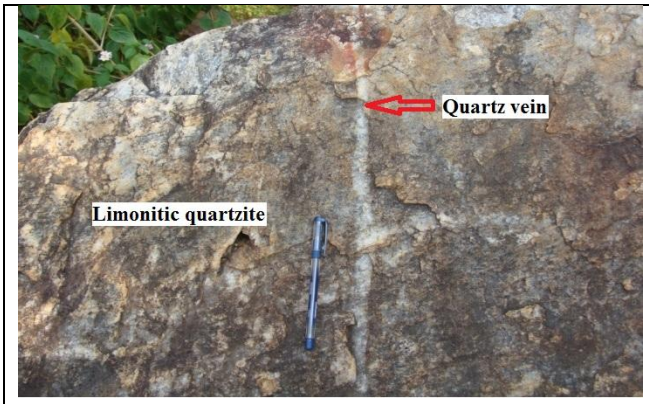


Fig. 2. (g) Field photograph showing quartz vein within limonitic quartzite.



Fig. 2. (h) Field photograph showing 2 sets of joint prominent.



Fig. 2. (i) Field photograph showing amphibolite.

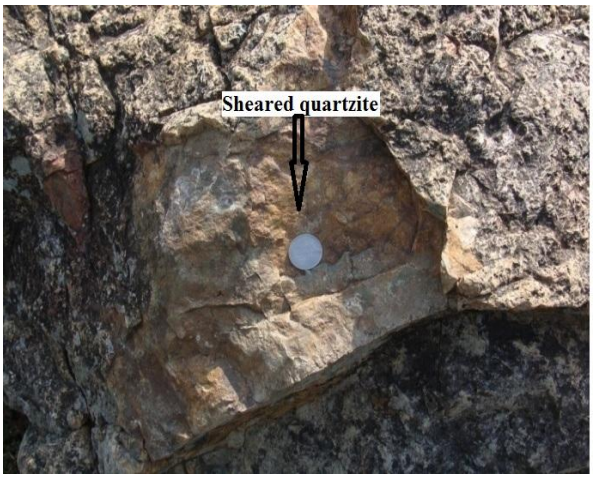


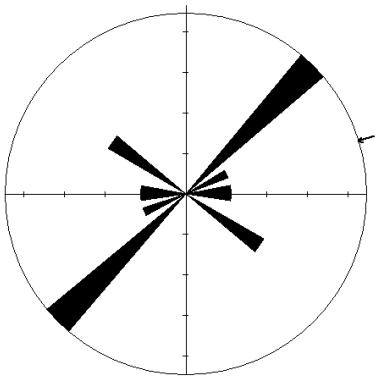
Fig. 2. (j) Field photograph showing sheared quartzite within Tamar Porapahar Shear Zone.



Fig. 2. (k) Field photograph showing 3 sets of joints.



Fig. 2. (l) Field photograph showing gold specks within quartzite.



Axial (non-polar) data
No. of Data = 9
Sector angle = 10°
Maximum = 44.4% [4 data]
Mean Resultant direction = 073-253

Fig. 3. (a) Rose diagram of joint azimuth showing three major joint orientations in the area.

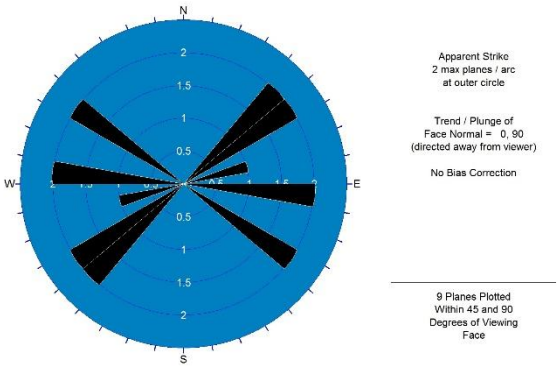


Fig. 3. (b) Apparent strike 2 max planes/ arc at outer circle are plotted.

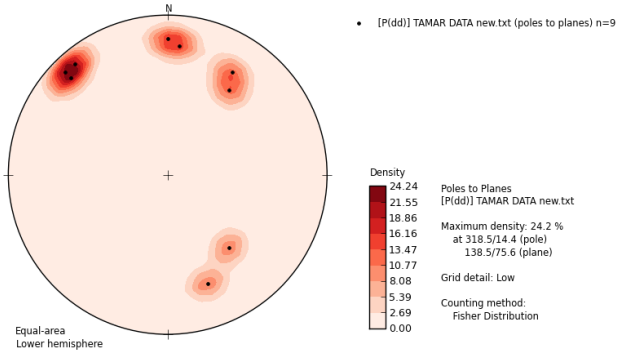


Fig. 3. (c) Beta diagram showing the pole position plotted in the stereonet.

5. Metamorphism and Alteration

Metamorphic mineral assemblages indicate greenschist to lower amphibolite facies conditions, with chlorite, biotite, muscovite, sericite, actinolite, and hornblende as characteristic phases. Retrograde alteration, including chloritization, sericitization, and carbonatization, is pervasive along shear zones and quartz veins, reflecting syn- to post-deformational fluid infiltration. Such metamorphic and alteration characteristics are typical of orogenic gold systems formed under mesothermal conditions at depths of ~5–15 km (Goldfarb et al., 2005; Groves et al., 2018). These are typical of orogenic gold systems and reflect fluid–rock interaction during deformation (Phillips et al., 1996; Groves et al., 2003). Carbonate alteration indicates CO_2-rich fluids, consistent with metamorphic devolatilization processes (Phillips and Powell, 2010).

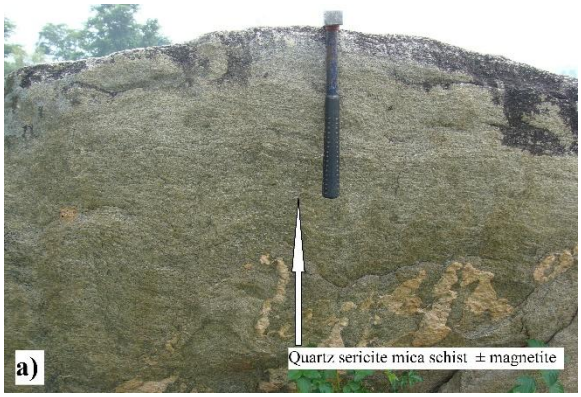


Fig. 4. (a) Field photograph showing Quartz sericite mica schist ± magnetite.

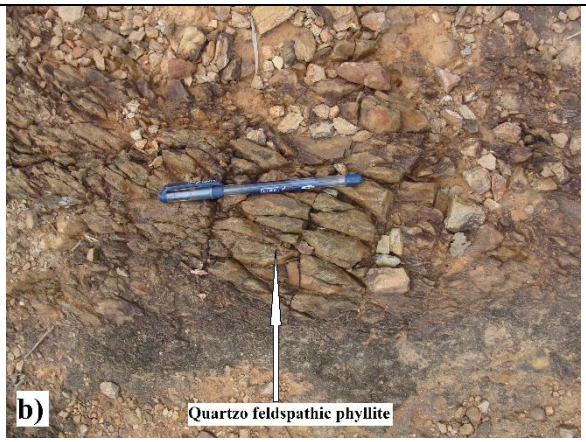


Fig. 4. (b) Field photograph showing Quartzo feldspathic phyllite.

6. Petrography and Ore Mineralogy

Native gold occurs as fine disseminations, inclusions, and thin sheets within quartzite and quartz veins, commonly associated with pyrite, arsenopyrite, chalcopyrite, and secondary goethite. Sulfides occur as disseminated grains and fracture-controlled aggregates, suggesting multiple stages of mineralisation and local remobilisation.

Quartz veins exhibit dynamic recrystallisation textures, including ribbon quartz, subgrain development, and polygonal grains, indicating deformation-assisted fluid flow and syn-tectonic vein formation. indicate deformation-assisted fluid flow and syn-tectonic mineralisation (Vearncombe et al., 1993; Kisters et al., 2003).



Fig. 5. (a) Hand specimen of quartzite containing specks of gold.



Fig. 5. (b) Hand specimen of limonitic quartzite containing specks of gold.

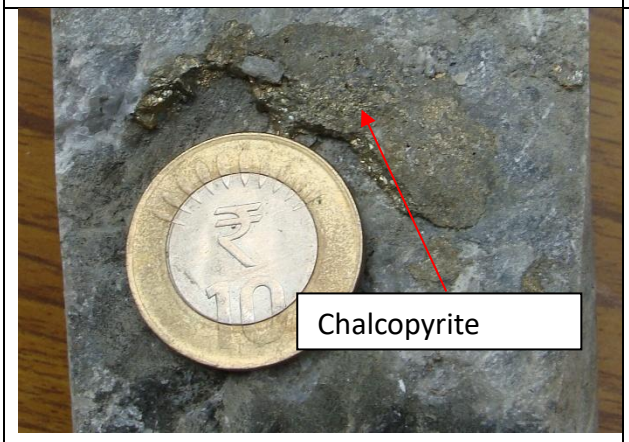


Fig. 5. (c) Core sample showing chalcopyrite.

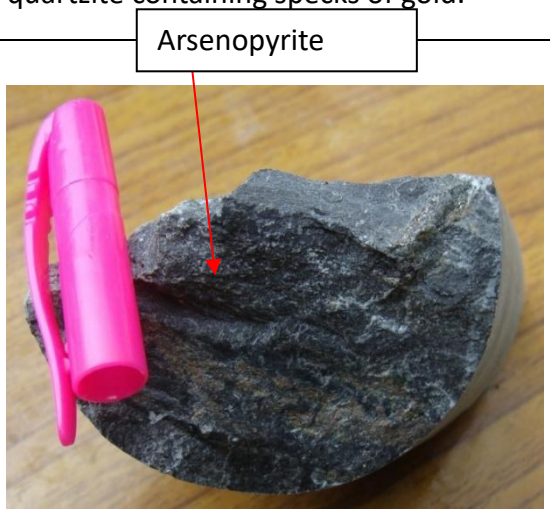


Fig. 5. (d) Core sample showing arsenopyrite.

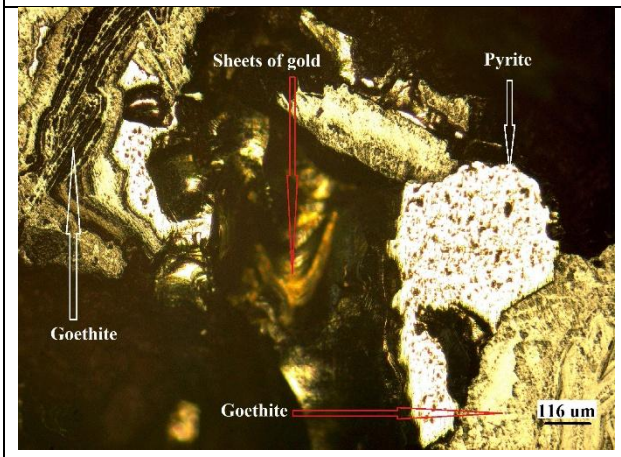


Fig. 5.(e) Polish section shows pyrite, goethite

and sheets of gold present within quartzite.

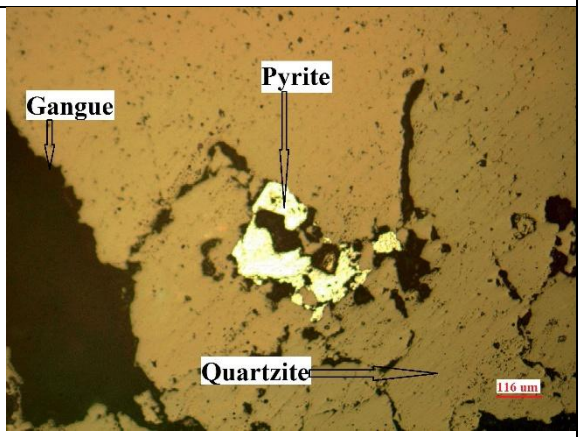


Fig. 5. (f) Polish section shows pyrite grains present within quartzite.



Fig. 6. (a) Petro micrograph showing ferruginous enrichment occur within phyllite.

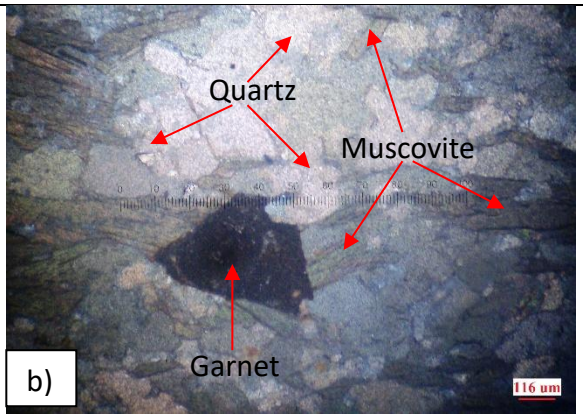


Fig. 6. (b) Petro micrograph showing bending of muscovite within mica schist.

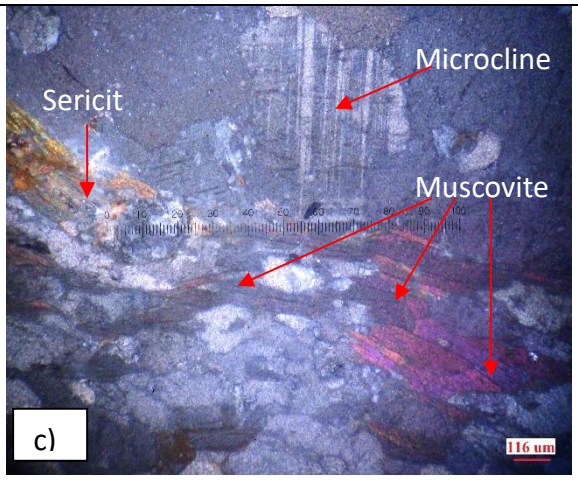


Fig. 6. (c) Petro micrograph section showing rotated muscovite present within quartz-sericite mica schist.

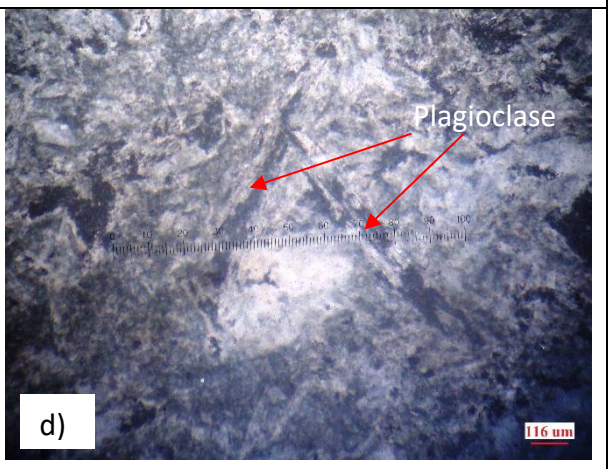


Fig. 6. (d) Petro micrograph showing plagioclase feldspar grains show ophitic texture present within tholeiitic lava.

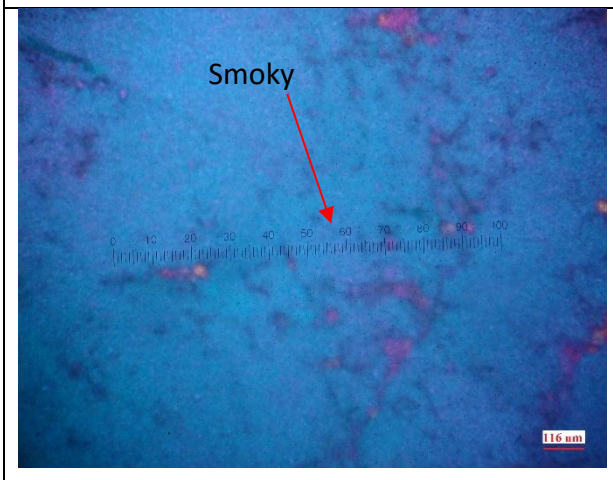


Fig. 6. (e) Petro micrograph showing smoky quartz (blue quartz) grains.

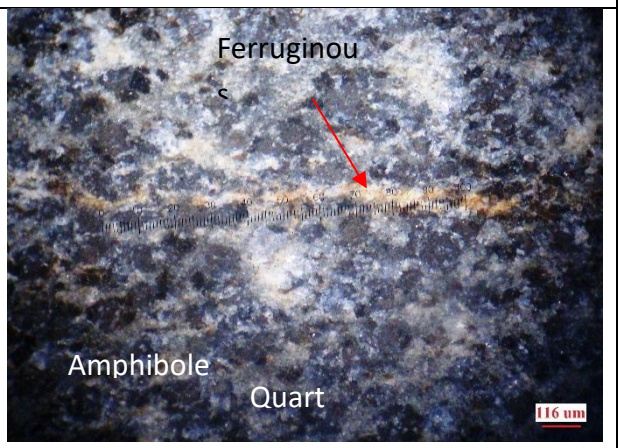


Fig. 6. (f) Petro micrograph showing some ferruginous enrichment present within amphibolite.

7. Whole-Rock Geochemistry

Quartzite and limonitic quartzite are characterised by high SiO_2 contents, whereas mica schist and amphibolite display enrichment in Al_2O_3, Fe_2O_3, MgO, and CaO. Geochemical discrimination diagrams indicate an active continental margin affinity for the supracrustal sequence, consistent with Paleoproterozoic convergent tectonics.

Chemical Index of Alteration (CIA) values of ~67–75 suggest moderate chemical weathering of source rocks and variable sediment maturity, supporting derivation from volcanic and volcaniclastic sources within a tectonically active orogenic environment. Trace element signatures indicate mafic contributions and hydrothermal alteration (Large et al., 2007; Goldfarb et al., 2010).

Sample	SiO_2	TiO_2	Al_2O_3	Fe_2O_3	MnO	MgO	CaO	Na_2O	K_2O	P_2O_5	Cr	Co	Ni	Cu	Zn	Total
Mica Schist	60.20	0.48	16.09	2.84	0.00	0.61	0.07	0.14	7.01	0.06	-	-	-	-	-	87.49
Quartzite	86.4	0.00	6.54	1.41	0.01	0.10	0.01	2.15	0.00	0.01	-	-	-	-	-	96.24
Ultramafics	45.05	0.01	8.60	15.58	19.02	0.18	8.81	0.28	0.05	0.13	128	82	63	28	109	98.81
Amphibolite	65.09	0.52	17.92	5.27	4.31	0.05	0.17	2.55	3.52	0.06	84	20	55	6	90	99.48

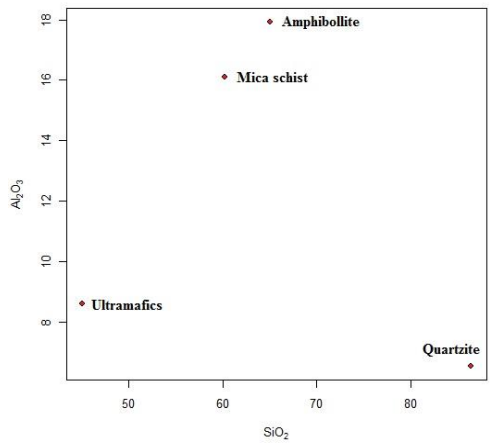


Fig. 7. (a) SiO_2 versus Al_2O_3 of the representative four samples are plotted in the X axis and Y axis respectively.

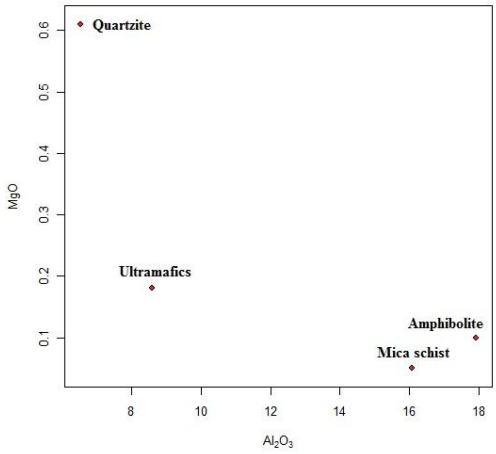


Fig. 7. (b) Al_2O_3 versus MgO are plotted in the X axis and Y axis respectively.

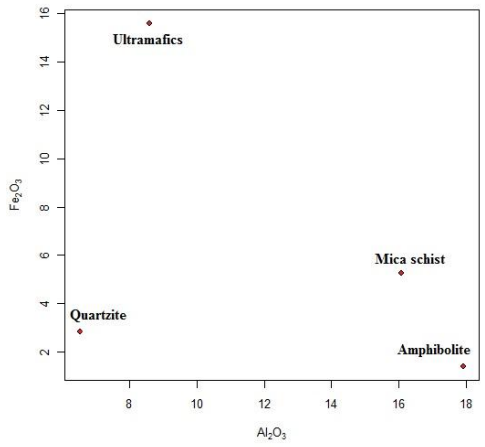


Fig. 7. (c) Al_2O_3 versus Fe_2O_3 are plotted in the X axis and Y axis respectively.

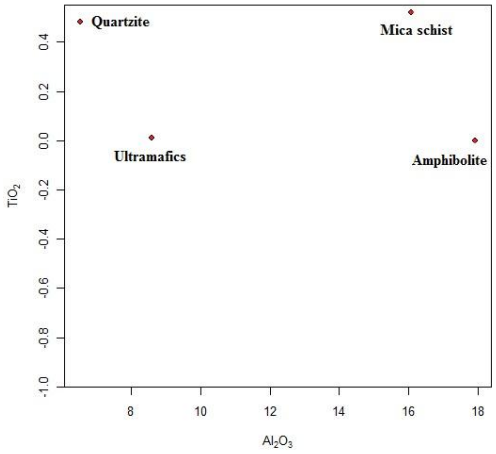


Fig. 7. (d) Al_2O_3 verses TiO_2 are plotted in the X axis and Y axis respectively.

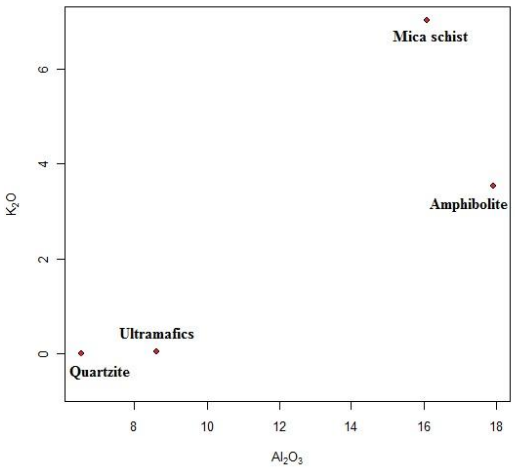


Fig. 7. (e) Al_2O_3 verses K_2O are plotted in the X axis and Y axis respectively.

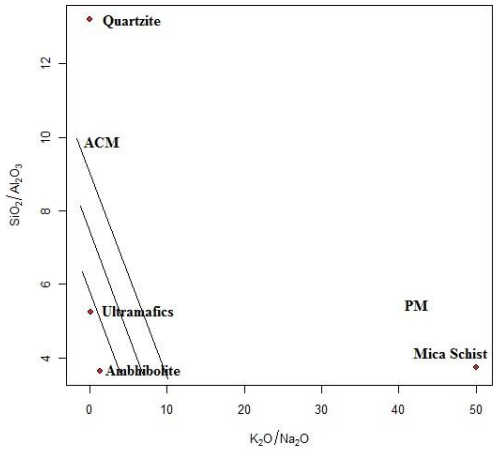


Fig. 7. (f) Tectonic discrimination diagram of Tamar area represented by the SiO_2/Al_2O_3-K_2O/Na_2O relations. The provenance fields of the representative four samples indicate to the Active Continental margin.

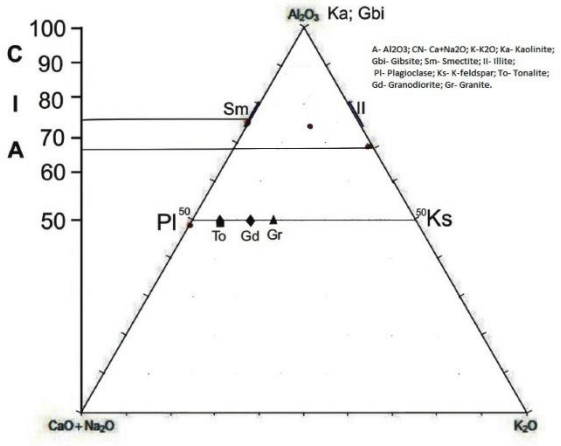


Fig. 7. (g) Calculated Chemical Index of Alteration (CIA) values for the Tamar and surrounding gold province.

8. Fluid Inclusion Characteristics

Fluid inclusions in auriferous quartz veins are dominated by aqueous–carbonic inclusions containing CO_2–CH_4–H_2O ± NaCl. Homogenization temperatures range from ~245 to 370 °C, and salinities are moderate, consistent with metamorphic fluids characteristic of orogenic gold systems.

Raman spectroscopic analyses confirm the presence of CO_2, CH_4, graphite, and minor H_2S, indicating reduced fluid conditions. The coexistence of CO_2 and CH_4 suggests fluid buffering by carbonaceous host rocks and redox reactions that facilitated gold precipitation through destabilization of gold–sulfur complexes (Roedder, 1984; Diamond, 2003; Burke, 2001; Frezzotti et al., 2012).

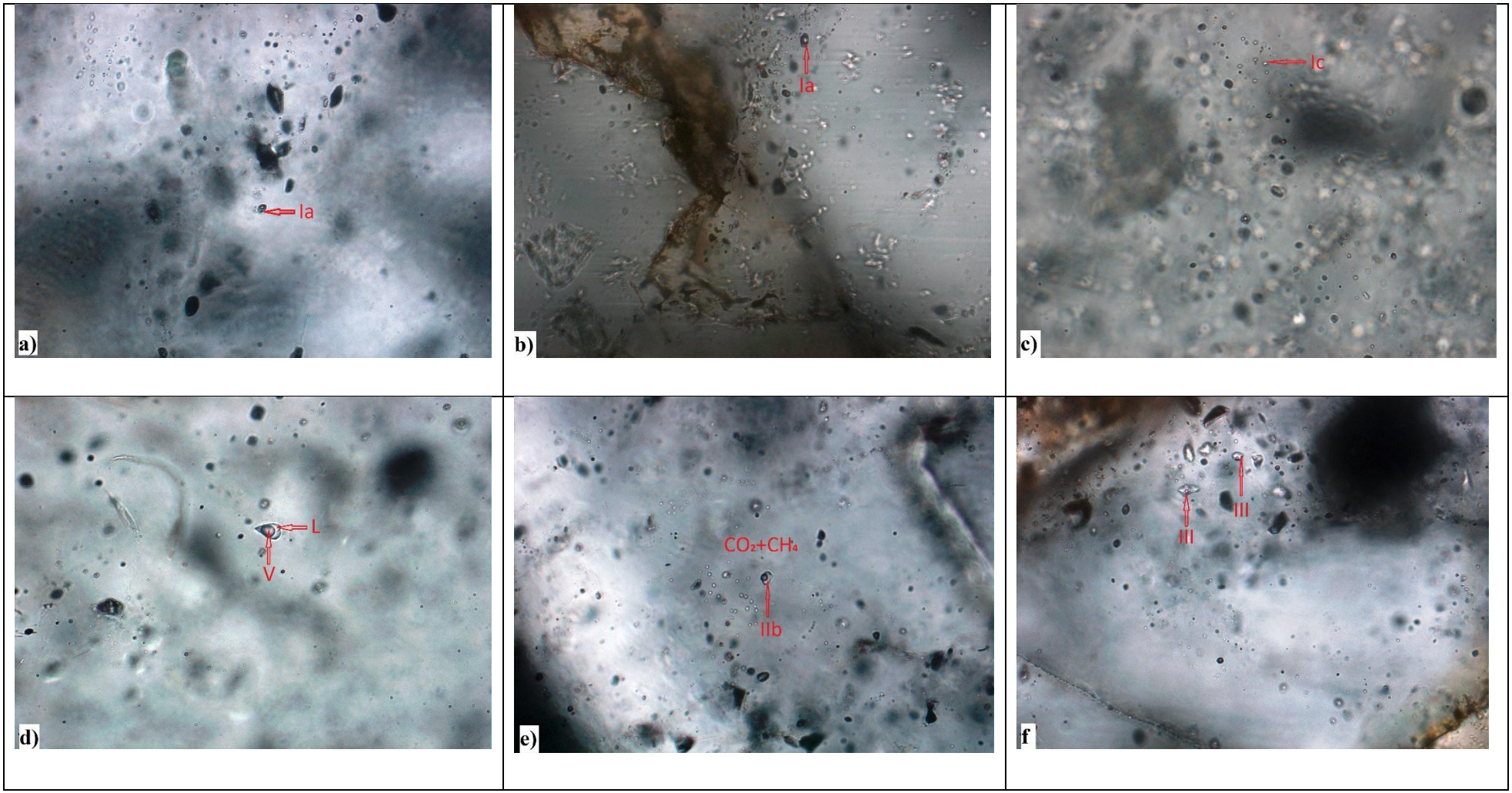


Fig. 8. Different types of fluid inclusions observed in the quartz veins of the Tamar gold deposit; (a) to (c) biphase aqueous-rich inclusions and (d) to (f) carbonic inclusions.

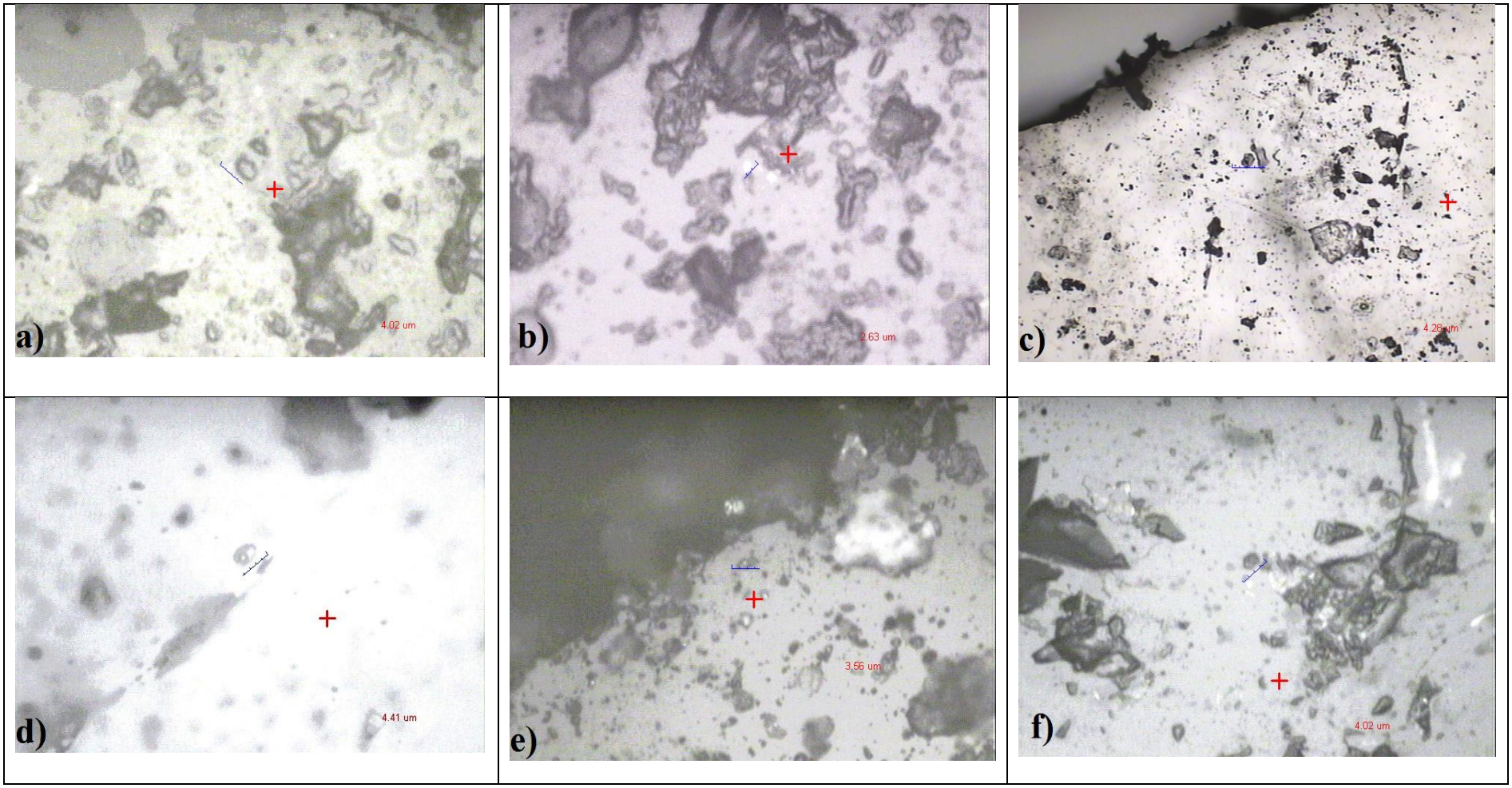
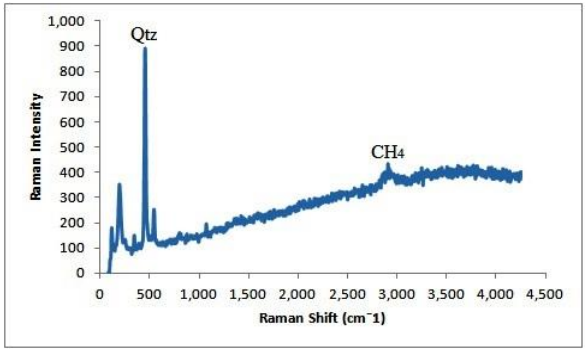
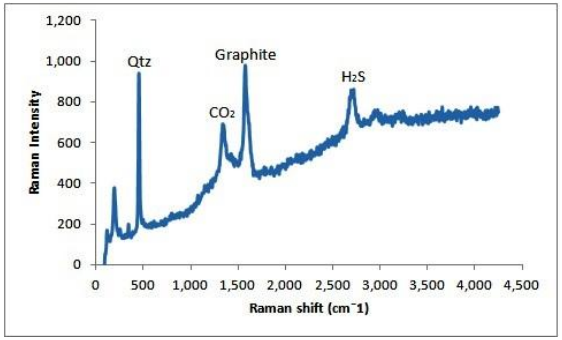


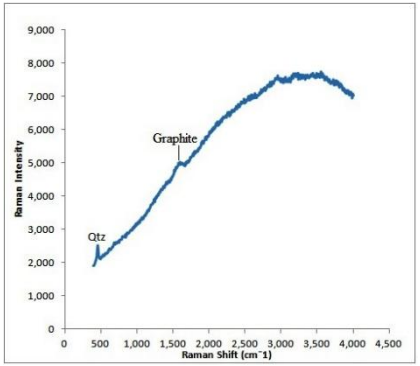
Fig. 9. (a), (b), (c), (d), (e) and (f) Different types of fluid inclusions present within quartzites, which are observed under Raman Spectrometry. Raman shift versus Raman intensity is plotted on the X axis and Y axis. Plotting the data of the above six pictures is given below, respectively.



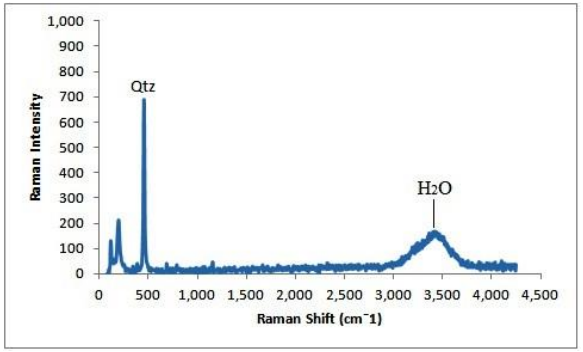
a) Raman shift of the fluid inclusions showing quartz and CH_4 peaks. (Burke, 2003).



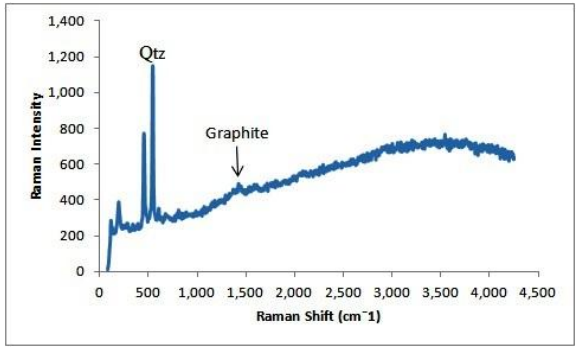
b) Raman shift of the fluid inclusions showing quartz, CO_2, Graphite and H_2S peaks. The carbonic inclusions indicate the strong reducing condition which favoured the precipitation of gold.



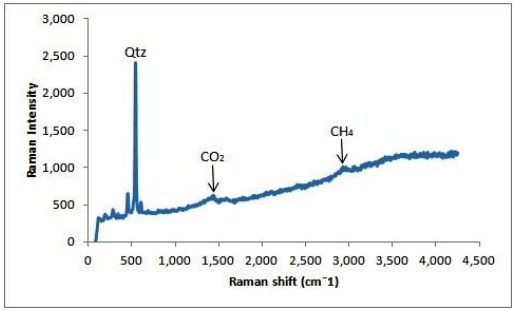
c) Raman shift of the fluid inclusions showing quartz and graphite peaks.



d) Raman shift of the fluid inclusions showing quartz and H_2O peaks.



e) Raman shift of the fluid inclusions showing quartz and graphite peaks.



f) Raman shift of the fluid inclusions showing quartz, CO_2 and CH_4 peaks. The carbonic inclusions indicate the strong reducing condition which favoured the precipitation of gold. Graphite was formed by the reaction between CH_4 and CO_2.

9. Nature and Controls of Mineralisation

An interplay of lithological reactivity and structural permeability controls gold mineralisation in the Tamar area. Reactive host rocks such as carbonaceous phyllite, limonitic quartzite, and amphibolite acted as chemical traps, whereas shear zones, foliation-parallel fractures, and extensional sites provided efficient fluid pathways.

Gold deposition occurred primarily during late-stage deformation in response to pressure fluctuations, fluid unmixing, and fluid–rock interaction. Mafic volcanic units are interpreted as a potential primary gold source, with subsequent remobilisation during regional metamorphism and deformation. Physicochemical Controls on Gold Precipitation occurs as Au–HS complexes in reduced fluids (Seward, 1997; Gammons and Williams-Jones, 1997). Precipitation is triggered by: (i) Fluid Immiscibility: CO_2–CH_4 separation reduces gold solubility (Ridley and Diamond, 2000; Gaboury, 2019), (ii) Sulfidation: Reaction with Fe-rich rocks destabilises Au complexes (Kerrich and Feng, 1992; Large et al., 2011), (iii) Redox Reactions: Interaction with carbonaceous rocks reduces fluid (Tomkins, 2010), (iv) Pressure Fluctuations: Fault-valve mechanism drives gold deposition (Weatherley and Henley, 2013)

10. Conclusions

Paleoproterozoic supracrustal rocks of the NSMB host gold mineralization in the Tamar area and is spatially associated with regional shear zones. Ore localisation is controlled by a combination of lithological reactivity and deformation-related permeability within WNW–ESE-trending ductile to brittle–ductile shear zones. Ore-forming fluids were aqueous–carbonic, reduced, and moderately saline, with homogenization temperatures of ~245–370 °C. Fluid inclusion and Raman data indicate CO_2–CH_4-rich fluids conducive to gold precipitation under mesothermal conditions. Gold precipitation occurred via: (a) fluid immiscibility (b) sulfidation (c) redox reactions. The Tamar gold system is best classified as an orogenic gold deposit formed during late Paleoproterozoic deformation. The study highlights the high metallogenic potential of the NSMB.

Acknowledgements

The authors are thankful to the Indian School of Mines for the facilities. The authors are also thankful to Mr Sashi Ranjan, Geologist, Geological Survey of India, Tamar Region, for the help and cooperation during the fieldwork. We would also extend my thanks to Prof. H. S. Pandalai, former Director (Finance & External Affairs), and Jr. Tech. Supdt. Shilpa V. Netravali, IIT Bombay, for Fluid Inclusion and Raman Spectrometry analysis. We also extend our thanks to the Director, ISM, HOD/AGL and Teachers-in-charge, XRF, Department of Applied Geology, ISM, Dhanbad, for the facilities.

Funding Declaration

"The authors declare that no specific funding was received for this research."

Ethics, Consent to Participate, and Consent to Publish

"Ethics, Consent to Participate, and Consent to Publish declarations: not applicable."

Data Availability Statement

All data generated or analysed during this study are included in this published article and its supplementary information files. These data were produced as part of the PhD work of the corresponding author. The corresponding author conducted the fluid inclusion and Raman spectrometry analyses at IIT Bombay, India, while the XRF data were generated under the guidance of the corresponding author at the Indian School of Mines, Dhanbad, India.

References

Bakker, R.J., 2003. Package FLUIDS: Computer programs for analysis of fluid inclusion data. *Chemical Geology* 194, 3–23.

Barker, S.L.L., Cox, S.F., 2011. Oscillatory zoning and trace element distribution in pyrite. *Geology* 39, 739–742.

Bierlein, F.P., Crowe, D.E., 2000. Phanerozoic orogenic lode gold deposits. *Reviews in Economic Geology* 13, 103–139.

Bierlein, F.P., Groves, D.I., Goldfarb, R.J., Dubé, B., 2006. Lithospheric controls on the formation of provinces hosting giant orogenic gold deposits. *Mineralium Deposita* 40, 874–886.

Bierlein, F.P., et al., 2009. Orogenic gold systems: Structure, scale and exploration. *Ore Geology Reviews* 35, 1–21.

Blewett, R.S., et al., 2010. Structural controls on orogenic gold deposits. *Precambrian Research* 183, 292–316.

Bodnar, R.J., 2003. Introduction to aqueous fluid inclusions. *Reviews in Mineralogy and Geochemistry* 32, 1–8.

Bohlke, J.K., 1982. Stable isotope geochemistry of hydrothermal fluids. *Economic Geology* 77, 168–185.

Burke, E.A.J., 2001. Raman microspectrometry of fluid inclusions. *Lithos* 55, 139–158.

Cox, S.F., 2005. Coupling between deformation and fluid flow in ore systems. *Economic Geology* 100, 39–75.

Cox, S.F., Knackstedt, M.A., Braun, J., 2020. Fault-valve behavior and episodic fluid flow. *Ore Geology Reviews* 116, 103231.

Craw, D., et al., 2015. Fluid flow and gold deposition in active orogenic belts. *Economic Geology* 110, 1–23.

Deng, J., Wang, Q., Santosh, M., 2019. Metallogenic provinces of gold. *Earth-Science Reviews* 190, 454–475.

Diamond, L.W., 2003. Introduction to fluid inclusions. *Reviews in Mineralogy and Geochemistry* 32, 1–8.

Dubé, B., Gosselin, P., 2007. Greenstone-hosted gold deposits. *Economic Geology* 100, 75–94.

Frezzotti, M.L., Tecce, F., Casagli, A., 2012. Raman spectroscopy in fluid inclusion studies. *Lithos* 154, 1–29.

Gaboury, D., 2019. Parameters for the formation of orogenic gold deposits. *Ore Geology Reviews* 106, 1–12.

Gammons, C.H., Williams-Jones, A.E., 1997. Chemical modeling of gold transport. *Geochimica et Cosmochimica Acta* 61, 1971–1983.

Goldfarb, R.J., Ayuso, R., Miller, M.L., et al., 2001. Timing of gold mineralisation. *Economic Geology* 96, 1–28.

Goldfarb, R.J., Baker, T., Dubé, B., Groves, D.I., Hart, C.J.R., Gosselin, P., 2005. Distribution, character, and genesis of gold deposits. *Economic Geology 100th Anniversary Volume*, 407–450.

Goldfarb, R.J., et al., 2010. Orogenic gold systems. *Economic Geology* 105, 1–25.

Goldfarb, R.J., Groves, D.I., Santosh, M., 2014. Orogenic gold and geodynamics. *Gondwana Research* 25, 26–43.

Goldfarb, R.J., Groves, D.I., 2015. Orogenic gold: Fluid and metal sources. *Lithos* 233, 2–26.

Goldfarb, R.J., Santosh, M., 2014. The dilemma of orogenic gold deposits. *Gondwana Research* 25, 1–10.

Groves, D.I., et al., 1995. Orogenic gold deposits: Classification and genesis. *Economic Geology* 90, 1–17.

Groves, D.I., Goldfarb, R.J., Knox-Robinson, C.M., 1998. Orogenic gold deposits. *Reviews in Economic Geology* 6, 17–34.

Groves, D.I., Goldfarb, R.J., Gebre-Mariam, M., Hagemann, S.G., Robert, F., 2003. Orogenic gold deposits: Unified model. *Economic Geology* 98, 1–27.

Groves, D.I., Santosh, M., Deng, J., Wang, Q., Yang, L., Zhang, L., 2018. Holistic model for orogenic gold deposits. *Ore Geology Reviews* 98, 124–148.

Groves, D.I., Goldfarb, R.J., Santosh, M., 2020. Secular distribution of gold deposits. *Economic Geology* 115, 729–744.

Groves, D.I., Santosh, M., 2015. Orogenic gold systems: Global perspective. *Gondwana Research* 27, 838–850.

Hagemann, S.G., Cassidy, K.F., 2000. Archean orogenic gold deposits. *Reviews in Economic Geology* 13, 9–68.

Hedenquist, J.W., Lowenstern, J.B., 1994. Role of magmas in hydrothermal systems. *Nature* 370, 519–527.

Henley, R.W., Ellis, A.J., 1983. Geothermal systems. *Earth-Science Reviews* 19, 1–50.

Hodkiewicz, P., et al., 2009. Structural evolution of gold systems. *Ore Geology Reviews* 35, 1–15.

Hronsky, J.M.A., Groves, D.I., Loucks, R.R., Begg, G.C., 2012. Mineral systems approach. *Ore Geology Reviews* 46, 1–13.

Kesler, S.E., 2005. *Ore-forming Fluids*. Society of Economic Geologists.

Kerrich, R., Feng, R., 1992. Hydrothermal alteration in gold deposits. *Geochimica et Cosmochimica Acta* 56, 2383–2397.

Kerrich, R., Goldfarb, R.J., Groves, D.I., Garwin, S., Jia, Y., 2000. Orogenic gold deposits. *Economic Geology* 95, 1–25.

Kisters, A.F.M., Groves, D.I., McNaughton, N.J., 2003. Timing of gold mineralisation. *Economic Geology* 98, 1–16.

Klein, C., 2001. Fluid inclusion petrography. *Reviews in Mineralogy* 32, 45–89.

Large, R.R., et al., 2007. Trace element signatures in pyrite. *Economic Geology* 102, 635–649.

Large, R.R., Bull, S.W., Maslennikov, V.V., 2011. Pyrite trace element chemistry. *Economic Geology* 106, 1–15.

McCuaig, T.C., Kerrich, R., 1998. P-T-t pathways in gold systems. *Ore Geology Reviews* 12, 1–28.

Mernagh, T.P., Wilde, A.R., 1989. Fluid inclusion geochemistry. *Chemical Geology* 75, 1–17.

Micklethwaite, S., Cox, S.F., 2010. Fault evolution and gold mineralisation. *Journal of Structural Geology* 32, 1350–1365.

Neumayr, P., Hagemann, S.G., Couture, J.F., 2008. Structural controls on gold deposits. *Ore Geology Reviews* 33, 1–23.

Phillips, G.N., Groves, D.I., Kerrich, R., 1996. Gold deposition mechanisms. *Ore Geology Reviews* 11, 1–24.

Phillips, G.N., Powell, R., 2010. Metamorphic devolatilization model. *Journal of Metamorphic Geology* 28, 689–718.

Phillips, G.N., et al., 2013. Gold systems evolution. *Economic Geology* 108, 1–23.

Pitcairn, I.K., Teagle, D.A.H., Craw, D., et al., 2014. Sources of fluids and metals. *Geochimica et Cosmochimica Acta* 125, 544–562.

Ridley, J.R., 1993. Gold transport mechanisms. *Economic Geology* 88, 1–12.

Ridley, J.R., Diamond, L.W., 2000. Fluid chemistry of gold deposits. *Reviews in Economic Geology* 13, 141–162.

Robert, F., Poulsen, K.H., Dubé, B., 2007. Classification of gold deposits. *Economic Geology*, 407–450.

Roedder, E., 1984. *Fluid Inclusions*. Reviews in Mineralogy 12.

Santosh, M., Groves, D.I., Zhang, L., 2017. Global synthesis of orogenic gold deposits. *Gondwana Research* 50, 1–19.

Seward, T.M., 1997. Metal transport in hydrothermal fluids. *Geochimica et Cosmochimica Acta* 61, 465–481.

Sibson, R.H., Robert, F., Poulsen, K.H., 1988. Fault-valve model. *Geology* 16, 551–555.

Tomkins, A.G., 2010. Sulfur degassing and gold deposition. *Geology* 38, 867–870.

Tomkins, A.G., Mavrogenes, J.A., 2001. Redox control on gold. *Geology* 29, 919–922.

Ueda, A., et al., 2002. Fluid inclusion constraints. *Economic Geology* 97, 1–15.

Vearncombe, J.R., Phillips, G.N., Reddy, S.M., 1993. Structural controls on gold. *Journal of Structural Geology* 15, 143–156.

Weatherley, D.K., Henley, R.W., 2013. Flash vaporization and gold deposition. *Geology* 41, 51–54.

Wilkinson, J.J., 2001. Fluid inclusions in ore deposits. *Lithos* 55, 229–272.

Yakymchuk, C., 2017. Partial melting and crustal evolution. *Earth-Science Reviews* 172, 1–24.

Zhai, M.G., Santosh, M., 2011. Precambrian tectonics. *Gondwana Research* 20, 299–311.

Supplementary Files

This is a list of supplementary files associated with this preprint. Click to download.

- Metadata.docx
- Table.docx